Journal of Zhejiang University-SCIENCE A (Applied Physics & Engineering)
ISSN 1673-565X (Print); ISSN 1862-1775 (Online)
www.jzus.zju.edu.cn; www.springerlink.com
E-mail: jzus@zju.edu.cn

Evaluation of the adhering layer ratio of iron ore granules and its influence on combustion-generated NO_x emission in iron ore sintering*

Hao ZHOU[†1], Ming CHENG[1], Jia-pei ZHAO[2], Ming-xi ZHOU[1], Zi-hao LIU[1]

[1]*State Key Laboratory of Clean Energy Utilization, Institute for Thermal Power Engineering, Zhejiang University, Hangzhou 310027, China*

[2]*Faculty of Maritime and Transportation, Ningbo University, Ningbo 315211, China*

[†]E-mail: zhouhao@cmee.zju.edu.cn; itpepc@gmail.com

Received Apr. 12, 2017; Revision accepted Sept. 27, 2017; Crosschecked May 9, 2018

Abstract: In iron ore sintering, the granulation process is the first and an important step. As the fine particles adhere to the coarse coke particles, the NO_x emission generated from coke combustion may be expected to be influenced by that adhering layer. In this study, the granule size distributions and adhering ratios were evaluated by a granulation model. Granulation experiments were also carried out to obtain the granule size distribution and adhering ratio. The influence of the adhering layer on NO_x emissions from the combustion of S type granules was studied by tube furnace experiments. Conclusions include: (1) The adhering ratio predicted from the granulation model can be used as a qualitative index for the evaluation of NO_x emission from coke combustion. (2) The influence of the adhering layer on NO_x emissions was enhanced with increasing adhering layer thickness of S type granules, and the NO_x reduction was enhanced at higher temperatures (around 1373 K), but weakened at lower temperatures (around 1173 K).

Key words: Iron ore sintering; Granulation; Adhering layer; Adhering ratio; NO_x emission
https://doi.org/10.1631/jzus.A1700193 **CLC number:** TK16

1 Introduction

The first step in iron ore sintering is the granulation of the mixture of iron ore, fluxes, and fuel to yield granules. During the granulation process, water and/or binding agents are used to cohere the fine particles to the coarser ones.

The addition of water and the properties of the iron ore, fluxes, and fuel particles will influence the formation of the adhering layer, and subsequently the NO_x emission from the combustion of coke particles in iron ore sintering.

In sintering, four granule types can be identified (Hida et al., 1982; Zhao et al., 2015) as shown in Fig. 1: S type (coarse coke particles covered by an adhering layer), P type (fine coke mixed with other fine solids e.g. iron ore and fluxes), C type (fine coke particles adhered to coarser ore or flux particles), and S′ type (single coke particles). The first three types are easily observable in the granulation products. The coke particles may exist in different positions in the granules, such as in the core or the adhering layer, because the coke particles are polydisperse. Zhao et al. (2015) simulated the influence of the adhering layer on oxygen diffusion during iron ore sintering, and showed that the adhering layer influenced both the coke combustion and the flame front properties. Teo et al. (1992) studied different coke addition methods, and concluded that the coke diameter had a greater influence on the granules than the properties

* Project supported by the National Natural Science Foundation of China (No. 51476137)
ORCID: Hao ZHOU, https://orcid.org/0000-0001-9779-7703; Ming CHENG, https://orcid.org/0000-0003-3253-6865

of the coke surface. Gan et al. (2015) studied the factors of granulation, and the proportion and specific surface area of the adhering fine powders, which would influence the permeability of the sinter bed. The coke particles were classified into three types: coarse particles (above 1 mm), intermediate particles (between 0.25 mm and 1 mm), and fine particles (smaller than 0.25 mm). It was found that the fine coke particles were almost always located in the adhering layers, while the coarser particles usually acted as the nuclei of granules. The distribution of the coke in granules influenced coke combustion behavior. For example, coke particles on the external surface are likely to increase the flame front speed, but decrease the sintering temperature and the heat accumulation in the iron ore sintering process.

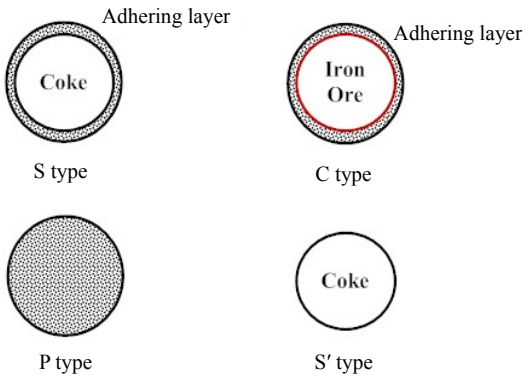

Fig. 1 Granule types commonly observed in granulation tests

In the S type granules, coke particles behave as the nuclei. The reaction of the hematite, limestone, and fine coke particles in the adhering layers decreases the ignition temperature, but the combustion rates are lower than those of coke particles produced by the coke late addition technique (Loo, 1991). The experiments by Kasai et al. (1992) demonstrated that if the adhering layers do not melt during combustion, the coke combustion rate and NO_x emission will be reduced. Sinter pot experiments demonstrated that NO_x release from S type granules was lower than that from the P and S′ types. Therefore, it is worthwhile investigating the structure and combustion behavior of S type granules.

In the granules commonly used in iron ore sintering, the percentage of coke particles above 1 mm exceeds 50% in weight, and the percentage of coke particles above 2 mm exceeds 30% in weight. Heterogeneous reactions can take place in the internal and external surfaces of the coke and also within the adhering layer of granules. Kasai et al. (1992)'s experiments demonstrated that when the coke was covered by unmelted raw materials, the coke combustion rate and the coke nitrogen conversion were decreased, but when the coke particles were covered by calcium ferrites, the oxygen could still diffuse to the coke surfaces as the calcium ferrites melted and flowed. This would increase the coke combustion rate and NO_x emission. However, it is believed that an appropriate amount of calcium ferrites can increase the combustion rate with low NO_x emission. There are many methods for NO_x reduction, for example, the application of a catalyst and the flue gas recirculation technique (Chen et al., 2008). Biomass char like rice husk can also be used to reduce the emission of NO_x, SO_x, and dust; however, the resulted sinter quality is usually lower (Mo et al., 1997; Gan et al., 2012; Kawaguchi and Hara, 2013). In another instance, Katayama and Kasama (2015) used the CaO to cover the coke particles to reduce NO_x emission and obtained higher sinter strength. Gan et al. (2014, 2016a) studied double-layered granules, the coke or biomass fuel was wrapped in the granules, and the granules were burnt under a low O_2 atmosphere, reducing the conversion of fuel-N to NO_x.

In this study, the granulation model was used to predict the size distributions of the granules and the values of adhering ratios, which are further compared with the experimental results. The influence of the adhering layer of S type granules on the NO_x emission from coke combustion was further studied by tube furnace experiments.

2 Experiment method and model

2.1 Raw materials and experiment method

The materials used include Australian ores AUS1, AUS2, and AUS3, Brazilian ores BRA1 and BRA2, limestone, dolomite, return fines, and coke. The size distribution of the ores is shown in Figs. 2 and 3 (Zhou et al., 2016) based on vibrating screen results. The fine particles under 250 μm were measured by a Malvern laser particle size analyzer and the mass mean diameters are shown in Table 1.

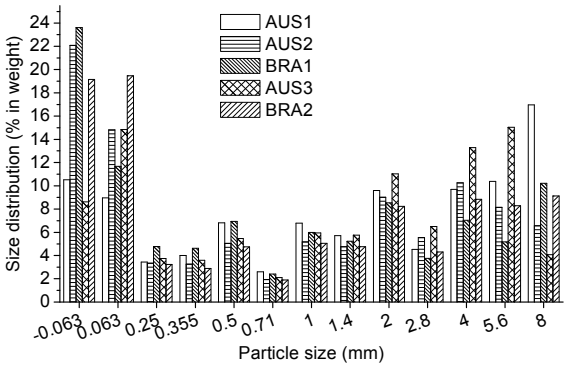

Fig. 2 Ores size distributions in the granulation tests

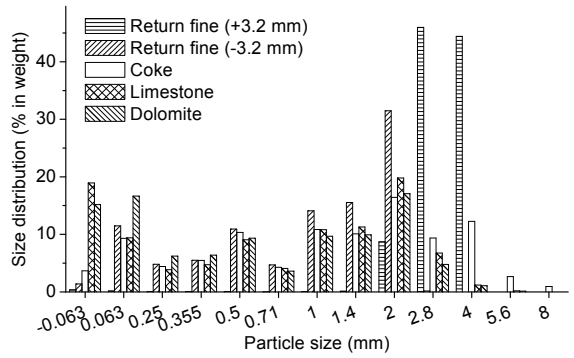

Fig. 3 Flux size distributions in the granulation tests

Table 1 Mass mean diameter $d_{k-0.25}$ of fine particles under 250 μm for the granulation tests

Ore	$d_{k-0.25}$ (μm)
AUS1	83.48
AUS2	56.99
AUS3	69.84
BRA1	77.39
BRA2	67.44
Return fine	112.13
Coke	178.71
Limestone	147.84
Dolomite	115.35

A drum granulator was used for granulation. The raw materials were first dry mixed in proportion for 1 min, and then wet mixed for 10 min. After granulation, the size distribution and the adhering ratio of the granules were measured.

For the adhering ratio measurement, the granules were frozen by liquid nitrogen, and then screened by the vibrating screen for 1 min. Each size fraction was then weighed, and the size distribution of the granules was obtained. Then the screened granules were put into a dry oven at 105 °C for 4 h. The subsequent steps included weighing the granules, wet screening the different size fractions of the granules, washing off the adhering layers under 250 μm, and drying the remaining nuclei particles. The dried nuclei particles were screened and the mass of different size fractions was recorded. The adhering ratio R is calculated based on the raw materials mass fraction of different size fraction W_i as

$$R=\frac{\sum(1-\alpha_i)W_i}{\sum\alpha_i W_i}, \tag{1}$$

where α_i is the nuclei particles ratio of size fraction i.

2.2 Granulation model

The granulation model proposed by Waters and Litster (Litster et al., 1986; Litster and Waters, 1988, 1990; Waters et al., 1989) is adopted in this study. The model predicts the final granule size distribution based on the particle size distribution of the raw materials based on a simplified population balance model. Assumptions of the model include:

1. Fine particles under 250 μm adhere to the coarse particles.

2. For a given ratio of fine particles to nuclei particles, the thicknesses of adhering layers are proportional to the size of the nuclear particles.

According to the granulation theory, the particles from size x to x+dx as nuclear particles would form granules of size x+2Δ(x) to x+dx+2Δ(x), where x is the raw materials particle size fraction, Δ(x) is the adhering layer thickness of size fraction x, and dx is the difference between two adjacent sizes. The nuclear particle ratio of size x is represented by $\alpha(x)$, the mass of the nuclei particles from size x to x+dx can be obtained by $\alpha(x)$, and the total granule mass of size x+2Δ(x) to x+dx+2Δ(x) can be expressed as the sum of two parts: the mass of nuclei particles from size x to x+dx, and the mass of adhering layer particles of size under 250 μm.

It is assumed that the adhering layer thickness Δ(x) is proportional to size x, and that x+2Δ(x) can be written as x+Ax, then the granule particle size distribution density function y_2 can be written as the product of the raw materials size distribution density function y_1 and $\alpha(x)$:

$$y_2(x+Ax)=y_1(x)\alpha(x)(1+KA), \tag{2}$$

where K and A are constants and K is related to properties of the raw materials. $\alpha(x)$ is the nuclei particles ratio of size fraction x, also known as the partition coefficient.

From experimental results, Litster concluded that $\alpha(x)$ can be represented as

$$\alpha(x)=\frac{1}{\sigma\sqrt{2\pi}}\int_{-\infty}^{\ln(x)}\exp\left[-\frac{\left(t-\ln(x_{0.5})\right)^2}{2\sigma^2}\right]\mathrm{d}t, \tag{3}$$

where σ=0.546; the calculation results are not sensitive to the value of σ, which was the mean value from Litster's experimental results.

For multicomponent mixtures, Eq. (3) can be derived from Eq. (1) in the discretized form as

$$y_2(x+2\Delta(x))=\alpha(x)(1+R)\sum_{k=1}^{m}(\delta_k y_k(x)), \tag{4}$$

where m is the number of raw materials, δ_k is the mass fraction of the raw materials k in the mixture on a dry basis, and $y_k(x)$ is the size distribution density function of the raw materials k in the mixture. Based on the mass conservation of adhering layer particles, the adhering ratio R can be written as

$$R=\frac{\int_0^{\infty}\sum_{k=1}^{m}(\delta_k y_k(x))(1-\alpha(x))\mathrm{d}x}{\int_0^{\infty}\sum_{k=1}^{m}(\delta_k y_k(x))\alpha(x)\mathrm{d}x}. \tag{5}$$

Eq. (5) can be discretized as

$$R=\frac{\sum_{i=1}^{n}\sum_{k=1}^{m}(1-\alpha_i)\delta_k\omega_{ik}}{\sum_{i=1}^{n}\sum_{k=1}^{m}\alpha_i\delta_k\omega_{ik}}, \tag{6}$$

where ω_{ik} is the mass fraction of raw materials k in size fraction i, α_i is the partition coefficient of size fraction i, and n is the number of size fractions of the raw materials. The adhering layer thickness and granule size can be calculated from R.

The important parameter in $\alpha(x)$ is $x_{0.5}$, which is a function of the saturation of the adhering layers and the mass mean diameter of the adhering particles. Saturation of the adhering layers is

$$S_l=\frac{1-\varepsilon_l}{\varepsilon_l}\frac{W_g}{\rho_{H_2O}V_{pl}}, \tag{7}$$

where ε_l is the porosity of the adhering layer, which is 0.315 according to Litster et al. (1986)'s results, ρ_{H_2O} is the water density, and V_{pl} is the volume of the adhering layer pores. W_g is the available granulation water (in mass), the total added water W_T minus the water adsorbed by particles:

$$W_g=W_T-\frac{\sum_{k=1}^{m}(\delta_k M_{ak})}{\sum_{k=1}^{m}(\delta_k/\rho_k)}, \tag{8}$$

where M_{ak} is the mass of water adsorbed by the raw materials k per unit mass, and ρ_k is the density of the raw materials k.

The mass mean diameter of the adhering layer particles d_l can be derived from $d_{k-0.25}$ and $\omega_{k-0.25}$. $d_{k-0.25}$ is the mass mean diameter of the particles under 250 μm for raw materials k, the $\omega_{k-0.25}$ is the mass fraction of the particles under 250 μm of raw materials k:

$$d_l=\frac{\sum_{k=1}^{m}\delta_k\omega_{k-0.25}\,d_{k-0.25}/\rho_k}{\sum_{k=1}^{m}\delta_k\,\omega_{k-0.25}/\rho_k}. \tag{9}$$

More details can be found from the related studies (Litster et al., 1986; Litster and Waters, 1988, 1990; Waters et al., 1989).

The interaction between particles in the adhering layers is the capillary force of the liquid, which influences the value of $x_{0.5}$. During granulation, the wall of the drum and the coarser particles will impact the adhering layer of granules. A proportion of large particles adhering to the granules would become adhering particles of another granules or become new nuclei; the size of these particles which act as nuclei or adhering particles with an equal chance is called $x_{0.5}$.

According to previous studies (Schubert et al., 1975; Kristensen et al., 1985), the tensile strength σ_t is expressed as

$$\sigma_t = 6S_l\left(\frac{1-\varepsilon}{\varepsilon}\right)\frac{\gamma_l \cos\theta}{d_l}, \quad (10)$$

where θ is the contact angle, γ_l is the surface tension, and ε is the porosity.

Then $x_{0.5}$ can be expressed as follows and fitted from the granulation experimental results:

$$x_{0.5} = f(S_l/d_l). \quad (11)$$

The calculation of the partition coefficient is as follows: the partition coefficient $\alpha(x)$ is assumed first, and then the value of $x_{0.5}$ is calculated. The Gauss integral is used to calculate the partition coefficient, and then to update $x_{0.5}$ and $\alpha(x)$ until the iteration criteria are achieved.

The water holding capacity of the particles was measured according to Litster's method. Approximately 100 g particles of size 2.0–2.8 mm were put into water for 10 min, and then taken out of the water. The surface water of the particles was absorbed on absorbent paper, and then the particles were weighed and put into an oven for 4 h at 105 °C. After that, the dried particles were weighed, and the water holding capacity can be obtained. Table 2 gives the water holding capacity of the ores used in this study.

In the granulation process, the real water holding capacity (WHC) is the values given in Table 2 minus the water content of the ore as received. The water absorbed by particles is less than the water holding capacity, and the relationship is given by Litster and Waters (1988) as

$$\text{Water absorbed} = \text{WHC} \times 0.854252 - 0.00559. \quad (12)$$

SMD is the Sauter mean diameter of the particles used. According to Eq. (9), the mean SMD of the mixture can be calculated by replacing $d_{k-0.25}$ with the SMD.

Then the adhering layer volume can be calculated by the adhering layer ratio, and the number of the adhering particles can be calculated by one of the following formulae:

$$\frac{R}{1+R}M_g = M_{ad}, \quad (13)$$

$$\frac{M_{ad}}{\rho_{mean}} = V_{ad}, \quad (14)$$

$$\frac{6V_{ad}}{\pi \times \text{SMD}_{mean}^3} = N_p, \quad (15)$$

where M_g is the total mass of granules, M_{ad} is the mass of adhering layers, ρ_{mean} is the mean density of the adhering layers, V_{ad} is the volume of the adhering layers, SMD_{mean} is the mean SMD of the adhering layer particles, and N_p is the number of the adhering layer particles. The effective surface of the adhering layer can be calculated by

$$N_p \times \pi \times \text{SMD}_{mean}^2 \times \varepsilon_l = A_{ad}, \quad (16)$$

where A_{ad} is the surface of the adhering layers. If M_g is set as 1 kg, Eq. (16) can be rewritten as

$$\frac{6R\varepsilon_l}{(1+R)\rho_{mean} \times \text{SMD}_{mean}} = A_{ad}. \quad (17)$$

Table 2 Water holding capacity (WHC) of the materials used in this study and Sauter mean diameter (SMD)

Ore	WHC (kg(H_2O)/kg)	SMD (μm)
AUS1	0.09297	6.149
AUS2	0.07685	3.580
AUS3	0.09841	3.637
BRA1	0.08054	4.118
BRA2	0.04975	12.394
Return fine	0.02430	19.059
Coke	0.20455	65.622
Limestone	0.04935	22.096
Dolomite	0.05183	13.685

3 Granulation experiments and calculation results

The experimental and model results are shown in Figs. 4–9. Test01 is the base condition with a water content of 6.29% in weight, as shown in Fig. 4. In Test02, the limestone content is increased and the water content is 6.68% in weight, as shown in Fig. 5. For Test03, the <0.5 mm coke particles are screened

out with water content of 6.54% in weight, as shown in Fig. 6. The <0.5 mm limestone particles are screened out at water content of 6.61% in weight in Test04, as shown in Fig. 7. To study the effect of return fines, the return fine content is decreased to 10% in weight at the water content of 6.72% in weight in Test05, as shown in Fig. 8. Considering the MgO on granulation, the MgO content is decreased in the sinter in Test06, i.e. the dolomite content of the granules is decreased at the water content of 6.49% in weight, as shown in Fig. 9. Table 3 shows the composition of materials for the base condition (dry basis). In our previous studies (Zhou et al., 2016, 2017), NO_x emissions at these conditions in the pilot tests were measured. Fig. 10 shows the partition coefficient obtained in the experiments. The materials noticeably influence the adhering layers. $x_{0.5}$ changes from 0.301 mm to 0.572 mm. The calculation results of the granule size distributions and the adhering ratios agree well with the granulation experiments, but there are some discrepancies. Possible reasons are: (1) the measurement of the water holding capacity

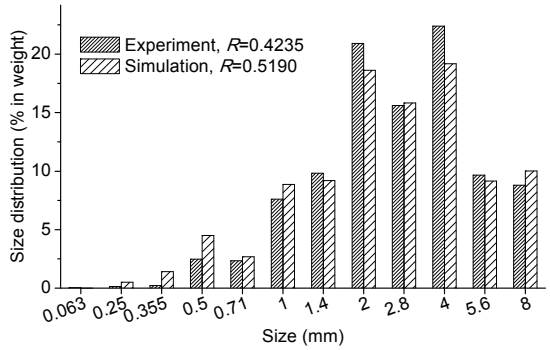

Fig. 4 Granule size distribution of the Test01 base condition

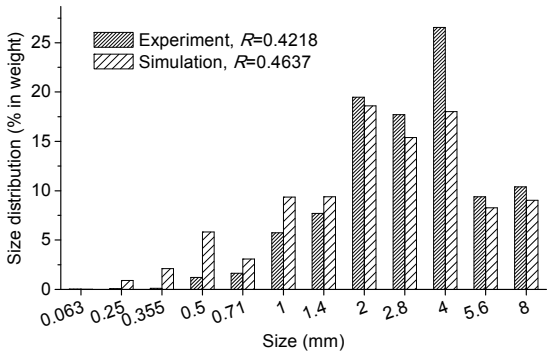

Fig. 5 Granule size distribution of Test02 with increased limestone content

Table 3 Sinter mix composition of the base condition (dry basis) with the aim moisture 6.5% in weight

Ore	Mass fraction (%)
AUS1	20.53
AUS2	10.26
AUS3	10.26
BRA1	10.26
BRA2	10.26
RF1	13.33
RF2	6.67
Coke	4.05
Limestone	9.11
Dolomite	5.25

RF1: 3.2–5.0 mm return fine particles; RF2: <3.2 mm return fine particles, actual water content 6.29% in weight

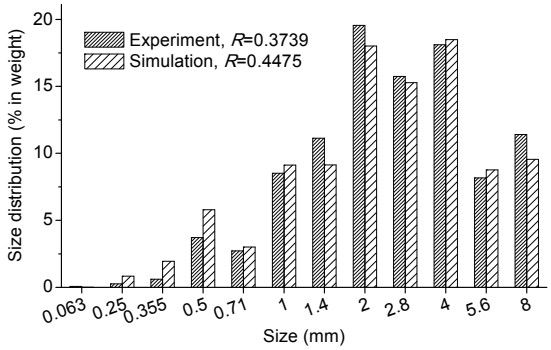

Fig. 6 Granule size distribution of Test03 with the removal of <0.5 mm coke particles

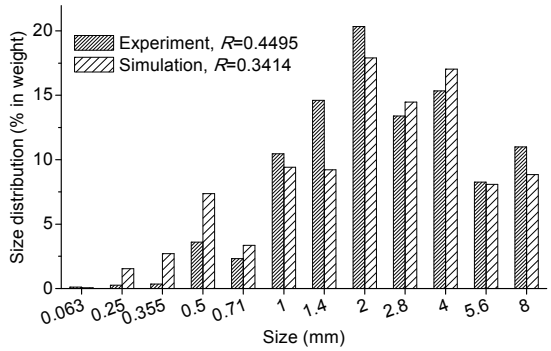

Fig. 7 Granule size distribution of Test04 with the removal of <0.5 mm limestone particles

may not be accurate enough, because the water on the irregular shape of the ore particles may not be fully taken up by the absorbent paper; (2) the adhering ratio measurement may carry some inaccuracy, as the adhering particles on the surface of the nuclei particles may not be cleaned up absolutely, or the nuclei particles may be broken up into finer particles during the

cleaning process. The areas of adhering layers from Test01 to Test06 are 14.50, 12.52, 16.99, 12.19, 16.31, and 13.45 (m^2/kg adhering layer), respectively. The area increased with the adhering ratio, but Test03 is an exception.

The SMD of coke fine particles is the maximum, so the SMD of the mixture will decrease if the coke fine particles are removed. More fine particles will increase the areas of adhering layers. According to previous study (Zhou et al., 2015), increasing the coke size decrease the NO_x emission. The increase of effective area may be one of the reasons.

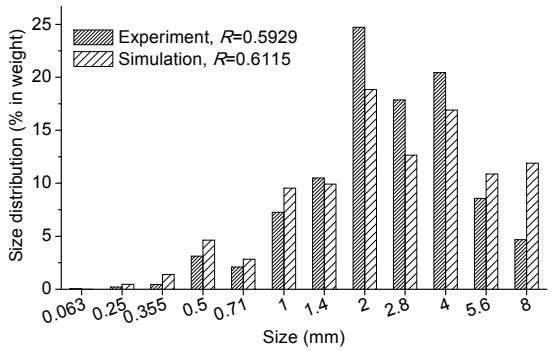

Fig. 8 Granule size distribution of Test05 with 10% return fine content in the sinter mix

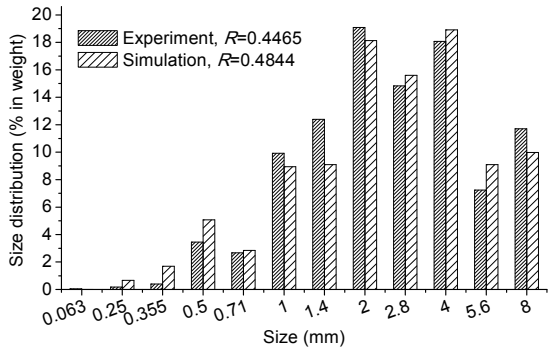

Fig. 9 Granule size distribution of Test06 with 1% MgO content in the sinter mix

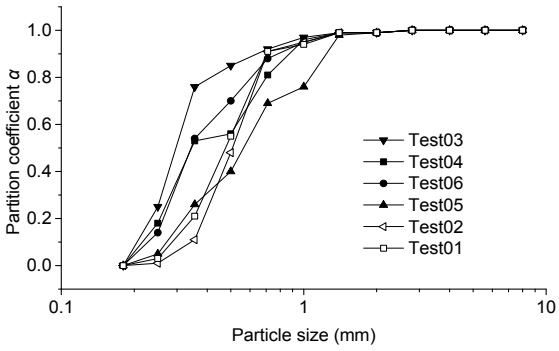

Fig. 10 Partition coefficient α obtained in the experiments

4 Influence of the adhering layer on NO_x emission

In granulation, the coke particles above 1 mm account for at least 50% in weight, which means that the coke particles are more likely to exist in S type granules. In order to analyze the influence of the adhering layers on the NO_x emission generated from coke combustion, tube furnace experiments were carried out. S type granules of different adhering ratios at different temperatures were studied. In Table 4, the first row is the proportion of fine particles under 0.25 mm in the size distribution of each material, and the second row is the mass of the materials used in the adhering layer.

Table 4 Proportion of fine particles in different ores size distributions and the added masses to the mixture

Ore	Proportion (% in weight)	Mass (g)
AUS1	19.48	0.292
AUS2	36.90	0.277
AUS3	23.45	0.176
BRA1	35.28	0.265
BRA2	38.63	0.290
Limestone	28.33	0.188
Dolomite	31.82	0.119
Return fine	12.84	0.188
Coke	12.98	0.038
Total		1.833

4.1 Tube furnace experiments

The materials used in the tube experiments included fine particles for the adhering layer and nuclei coke particles (2.0–2.8 mm). An Alicat air flow meter was used to accurately control the air flow rate used in the tests. A Testo 350 gas analyzer was used for measuring the gas composition. The experiments were carried out in a tube furnace.

The experimental procedures were as follows:

Step 1: The fine particles shown in Table 4 were used for the formation of the adhering layers. The fine particles were adhered to the nuclei coke particles by

water. The proportions of different ore fines were adopted according to the proportion of fine particles in each size distribution of the raw materials and the materials ratios in the base condition of Table 3. Table 5 shows the proximate analysis and ultimate analysis of the coke.

Step 2: Before the tube furnace experiments, the granules were dried in the oven at 105 °C for 4 h.

Step 3: The granules were put into the tube furnace with the preheating temperatures of 1173 K and 1373 K, respectively. The air flow rate was 4 NL/min, and the gas analyzer was connected to the outlet of the tube furnace.

Table 5 Ultimate and proximate analyses of coke

Item	Mass fraction (% in weight)
Proximate analysis	
M_{ad}	1.12
A_{ad}	13.42
V_{ad}	1.61
FC_{ad}	83.35
M_t	12.02
Ultimate analysis	
C_{ad}	83.26
H_{ad}	1.05
N_{ad}	1.10
$S_{t,ad}$	0.71
O_{ad}	0.39

The total mass of the fine particles remained unchanged, while the mass of nuclei coke particles changed to produce adhering layers of different thickness. Two adhering ratios were produced as 1.83/2 and 1.83/3. According to these adhering ratios, about 1 g of coke nuclei particles with additional adhering layers were prepared as the samples, which meant the samples were 1.9 g for the adhering ratio of 1.83/2 and 1.6 g for the adhering ratio of 1.83/3. The experimental system is shown in Fig. 11.

In the following, the NO_x emissions and the char nitrogen conversions were calculated. NO_x emission (mg) is

$$M=\frac{Q}{60}\sum m_{\mathrm{NO}_x}\times 10^{-6}\times\frac{1}{22.4}\times M_{\mathrm{NO}}\times 1000,$$

and coke nitrogen conversion C_{CN} is

$$C_{\mathrm{CN}}=\frac{M}{W_{\mathrm{cg}}\times \mathrm{N_{ad}}}\times\frac{M_{\mathrm{N}}}{M_{\mathrm{NO}}},$$

where Q is the volume flow rate, $\sum m_{\mathrm{NO}_x}$ is the sum of the NO_x emissions from the start to the end, M_{NO} is the molecular weight of NO, W_{cg} is the coke mass in the granules, M_N is the nitrogen atomic weight, and N_{ad} is the nitrogen content shown in Table 5.

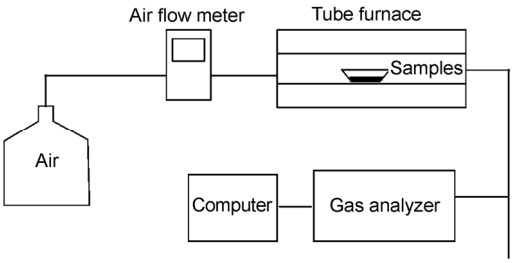

Fig. 11 Tube furnace experiment system used in this study

4.2 Experimental results and discussion

Six sets of experimental results were obtained. Fig. 12 shows the NO_x emissions of granules and coke at 1173 K. Fig. 13 shows the NO_x emissions of granules and coke at 1373 K. The calculated results are shown in Table 6, where CNC stands for char nitrogen conversion, and AR stands for adhering ratio. The calculated effective areas of the adhering layers are respectively 16.08 m^2/kg (R=1.83/3) and 20.28 m^2/kg (R=1.83/2).

It is seen from Table 6, Fig. 12, and Fig. 13 that there is no significant difference between the NO_x emissions from coke at different temperatures. The total NO_x emissions of coke at the two temperatures were close to each other, but the peak value of NO_x emission was lower when coke was at 1173 K, and the peak time of NO_x emission in Fig. 12c is longer than the peak time of NO_x emission in Fig. 13c. It is seen that the preheating temperature can influence the coke combustion rate.

The adhering layers of the granules reduced the time of the NO_x emission peak, especially at a temperature of 1373 K, and the total NO_x emissions were reduced as well. However, the NO_x emissions increased at a temperature of 1173 K. It is seen that the adhering layers had a great influence on coke particle combustion. The combustion of coke particles with

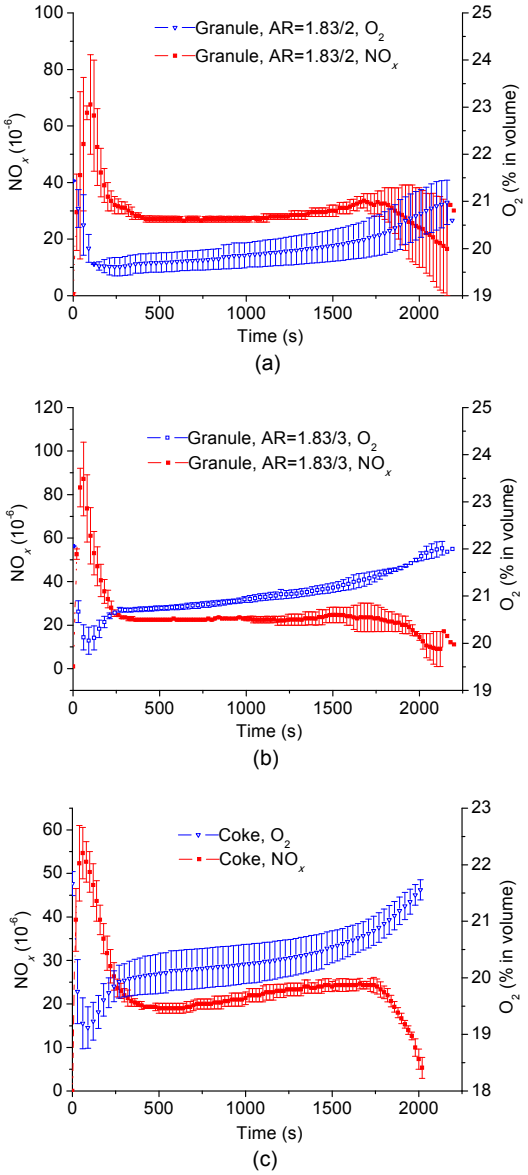

Fig. 12 NO_x emissions and O_2 from granules with the AR of 1.83/2 (a) and 1.83/3 (b) and from the combustion of coke (c) at 1173 K

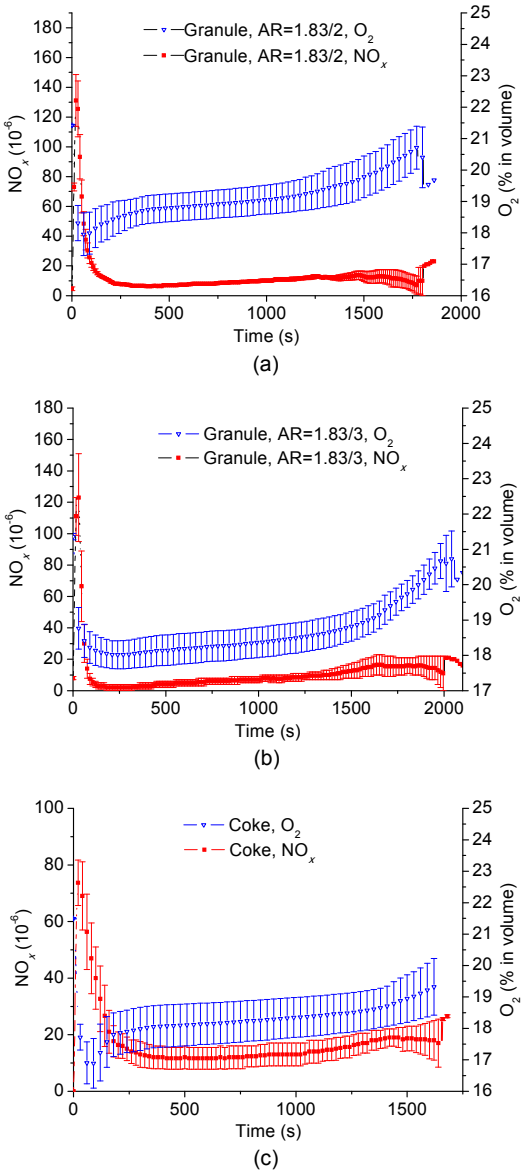

Fig. 13 NO_x emissions and O_2 from granules with the AR of 1.83/2 (a) and 1.83/3 (b) and from the combustion of coke (c) at 1373 K

Table 6 NO_x emissions from the experiments involving coke and granules with different adhering layer ratios

Item	1173 K		1373 K	
	NO_x (mg)	CNC (% in weight)	NO_x (mg)	CNC (% in weight)
Granules (AR=1.83/2)	6.11±1.390	25.44±5.79	2.25±0.60	9.43±2.51
Granules (AR=1.83/3)	4.84±0.032	20.15±0.13	2.86±0.20	11.98±0.84
Coke	4.25±0.275	18.00±1.17	4.22±0.32	17.88±1.36

adhering layers would take a longer time, especially at lower temperatures. Kasai and Omori (1986) studied the combustion rates of S and P types quasi particles formed by coke and alumina particles. Their results showed that the adhering layer decreases the combustion rate.

From the above results, it is concluded that NO_x reduction for granules was promoted at higher temperatures. NO_x was mainly from the nitrogen in the form of coke-N, and the NO_x was reduced for the heterogeneous reaction with the active site at the surface of coke. According to the results of Kasai et al. (1992) in the early stage of coke combustion, the NO_x emission is high because of the low temperature of the coke surface, and the combustion rate should be depressed to lower NO_x emission. Our results showed the same trend. The NO_x emission was initially high, but then dropped towards to a certain stable value. The peak values of NO_x from granules were higher than from the coke under the same conditions. The possible reason was that the adhering layer hindered the surrounding radiation, lowered the coke surface temperature. However, at the same time, at higher preheating temperature the peak values were higher, and it is possible that more cokes combust at the temperature of 1373 K.

According to the results of Kasai et al. (1992) the calcium ferrite in the adhering layer can melt and the melts move away from the coke surface at 1273 K. After that, the combustion rate will not decrease too much and the NO_x emission will be lowered.

Generally, the granule was composed of a porous adhering layer and a porous coke particle, and the product gas from the coke combustion and air cannot diffuse easily in the granule. More heterogeneous reactions will occur on the particle surface. The first step of the heterogeneous reaction is generally the dissociative adsorption of NO at the free carbon sites at low temperature as (Pevida et al., 2007)

$$C\ (\text{active site})+(NO)_2 \rightarrow 2C(N)+C(O_2).$$

Pevida et al. (2007) studied the mechanism of the NO-char heterogeneous reaction, and showed that temperature plays an important role. The product gases of the char gasification between 750 °C and 1000 °C were N_2 and CO_2. The whole reactions are as follows (Pevida et al., 2007):

$$2C\ (\text{active site})+NO \rightarrow C(N)+C(O),$$
$$C(N)+NO \rightarrow N_2+C(O),$$
$$C\ (\text{active site})+C(O)+NO \rightarrow C(O_2)+C(N),$$
$$C(O_2) \rightarrow CO_2+C\ (\text{active site}).$$

The experimental results showed that the NO_x emission from granules increased at 1173 K, as compared with the NO_x emission from coke combustion. NO_x emission from the AR=1.83/2 condition was more than that from AR=1.83/3 condition. The possible reason is that more coke surfaces were covered by the unmelted adhering layers, and the unmelted particles covered the coke surface and reduced the first heterogeneous reactions. The $CaCO_3$ began to transform to CaO and CO_2 at 795 K (Yang and Standish, 1991), and at the melting point of the $CaO\text{-}Fe_2O_3$ system (1373 K), the calcium ferrites formed and flowed. Thus, at the preheating temperature of 1373 K, more calcium ferrites surrounding the fine coke particles in the adhering layer were melted. NO_x emission, therefore, decreased due to the presence of the melted calcium ferrites. The NO_x emission from the AR=1.83/2 condition was less than that from the AR=1.83/3 condition. This is probably due to the formation of more calcium ferrites in the thicker adhering layer. At higher preheating temperature, it would be more effective to reduce NO_x emission by depressing the coke combustion rate at the early combustion stage.

In our previous study (Zhou et al., 2015), it was found that high temperature can increase the conversion of coke–N to NO_x, and NO_x reduction as well. According to our results, the main reason for the increasing NO_x reduction is the melt formed in the adhering layer. Morioka et al. (2000) studied the effect of the mixture of CaO and iron oxides (FeO+CaO, Fe_2O_3+CaO, and Fe_3O_4+CaO) on NO_x reduction. It was found that calcium ferrite was useful for NO_x reduction, especially at low oxygen potential. Fan et al. (2015) and Gan et al. (2016b) studied the effect of the flue gas recirculation on NO_x reduction. They found that the elimination of NO_x was the most efficient in the sinter zone at 700 °C, where the sinter zone worked as a catalyst for the NO-CO reaction.

From our results, the thicker adhering layer of the S type granules is found to have two conflicting effects. NO_x was found to increase at lower temperatures due to thicker adhering layers but to decrease at higher temperature due to thicker melts. In Section 3, the average thickness of the granules was calculated which can be used as an index for NO_x emission in iron ore sintering. According to our previous studies (Zhou et al., 2015, 2016), the NO_x emission from a

pilot scale sinter pot was affected by the temperature, and the NO_x can be decreased by 5% to 10% in volume with the removal of the <0.5 mm coke particles, because NO_x was reduced in the pores of coke particles and more coke particles were available as nuclear particles. Increasing water addition will increase the adhering layer thickness of granules and also the NO_x emission in the upper layer, but it will decrease the NO_x emission in the lower layer. The char nitrogen conversion from the coke combustion remained almost constant at 18% in weight for different temperatures. While the adhering layer influenced the coke combustion rate and NO_x emission, the coke nitrogen conversion of the granules with AR=1.83/2 was around 25% in weight, which was higher than for the granules with AR=1.83/3 by about 5% at 1173 K, and both were higher than coke combustion at the same temperature. At 1373 K, the coke nitrogen conversion of the granules with AR=1.83/2 was approximately 9% in weight, which was lower than the granules with AR=1.83/3 by about 2% at 1373 K, and both were lower than the coke combustion at the same temperature.

Based on the above discussion, it is preferable to form granules with thinner adhering layers in the upper layer of the sinter bed, but with thicker adhering layer in the lower bed. This is proposed based on the fact that the upper layer temperature of the sinter bed was lower as the air in the upper bed is not well preheated. As for a sinter plant, the flue gas recirculation is a useful method for NO_x reduction since the NO_x in flue gas can be reduced in the sinter zone.

5 Conclusions

In this study, Litster's granulation model was used to calculate the size distribution, the adhering layer ratio of the granules, and the effective area of the adhering layer produced in the granulation process. Experiments were conducted to validate the granulation model. The modeling results were found to agree qualitatively with the experimental results.

The experimental results showed that the influence of the adhering layer on NO_x emission during coke combustion was obvious at both high and low temperatures. The thicker adhering layer has a greater influence for the S type granules during sintering at both low and high temperatures. NO_x emission increases with the thicker adhering layer at lower temperatures but decreases at higher temperatures. This means the influence of adhering layer thickness on NO_x emissions is as important as temperature.

References

Chen YG, Guo ZC, Wang Z, 2008. Application of modified coke to NO_x reduction with recycling flue gas during iron ore sintering process. *ISIJ International*, 48(11):1517-1523. https://doi.org/10.2355/isijinternational.48.1517

Fan XH, Yu ZY, Gan M, et al., 2015. Elimination behaviors of NO_x in the sintering process with flue gas recirculation. *ISIJ International*, 55(10):2074-2081. https://doi.org/10.2355/isijinternational.ISIJINT-2015-180

Gan M, Fan XH, Chen XL, et al., 2012. Reduction of pollutant emission in iron ore sintering process by applying biomass fuels. *ISIJ International*, 52(9):1574-1578. https://doi.org/10.2355/isijinternational.52.1574

Gan M, Fan XH, Ji ZY, et al., 2014. Effect of distribution of biomass fuel in granules on iron ore sintering and NO_x emission. *Ironmaking & Steelmaking*, 41(6):430-434. https://doi.org/10.1179/1743281213Y.0000000138

Gan M, Fan XH, Ji ZY, et al., 2015. Optimising method for improving granulation effectiveness of iron ore sintering mixture. *Ironmaking and Steelmaking*, 42(5):351-357. https://doi.org/10.1179/1743281214Y.0000000237

Gan M, Fan XH, Lv W, et al., 2016a. Fuel pre-granulation for reducing NO_x emissions from the iron ore sintering process. *Powder Technology*, 301:478-485. https://doi.org/10.1016/j.powtec.2016.05.043

Gan M, Fan XH, Yu ZY, et al., 2016b. A laboratory-based investigation into the catalytic reduction of NO_x in iron ore sintering with flue gas recirculation. *Ironmaking & Steelmaking*, 43(6):442-449. https://doi.org/10.1080/03019233.2015.1136114

Hida Y, Sasaki M, Enokido T, et al., 1982. Effect of the existing state of coke breeze in quasi-particles of raw mix on coke combustion in the sintering process. *Tetsu to Hagane-Journal of the Iron and Steel Institute of Japan*, 68(3):400-409 (in Japanese). https://doi.org/10.2355/tetsutohagane1955.68.3_400

Kasai E, Omori Y, 1986. Combustion-rate of coke at different existing states prepared by fine alumina. *Tetsu to Hagane-Journal of the Iron and Steel Institute of Japan*, 72(10): 1537-1544 (in Japanese). https://doi.org/10.2355/tetsutohagane1955.72.10_1537

Kasai E, Wu SL, Sugiyama T, et al., 1992. Combustion-rate and NO emission during combustion of coke granules in packed-beds. *Tetsu to Hagane-Journal of the Iron and Steel Institute of Japan*, 78(7):1005-1012 (in Japanese). https://doi.org/10.2355/tetsutohagane1955.78.7_1005

Katayama K, Kasama S, 2015. Influence of lime coating coke on NO_x concentration in sintering process. *Tetsu to Hagane-Journal of the Iron and Steel Institute of Japan*,

101(1):11-18 (in Japanese). https://doi.org/10.2355/tetsutohagane.101.11

Kawaguchi T, Hara M, 2013. Utilization of biomass for iron ore sintering. *ISIJ International*, 53(9):1599-1606. https://doi.org/10.2355/isijinternational.53.1599

Kristensen HG, Holm P, Schaefer T, 1985. Mechanical-properties of moist agglomerates in relation to granulation mechanisms part II. Effects of particle-size distribution. *Powder Technology*, 44(3):239-247. https://doi.org/10.1016/0032-5910(85)85005-1

Litster JD, Waters AG, 1988. Influence of the material properties of iron-ore sinter feed on granulation effectiveness. *Powder Technology*, 55(2):141-151. https://doi.org/10.1016/0032-5910(88)80097-4

Litster JD, Waters AG, 1990. Kinetics of iron-ore sinter feed granulation. *Powder Technology*, 62(2):125-134. https://doi.org/10.1016/0032-5910(90)80075-A

Litster JD, Waters AG, Nicol SK, 1986. A model for predicting the size distribution of product from a granulating drum. *Transactions of the Iron and Steel Institute of Japan*, 26(12):1036-1044. https://doi.org/10.2355/isijinternational1966.26.1036

Loo CE, 1991. Role of coke size in sintering of a hematite ore blend. *Ironmaking & Steelmaking*, 18(1):33-40.

Mo CL, Teo CS, Hamilton I, et al., 1997. Admiring hydrocarbons in raw mix to reduce NO_x emission in iron ore sintering process. *ISIJ International*, 37(4):350-357. https://doi.org/10.2355/isijinternational.37.350

Morioka K, Inaba S, Shimizu M, et al., 2000. Primary application of the "In-Bed-deNOx" process using Ca-Fe oxides in iron ore sintering machines. *ISIJ International*, 40(3):280-285. https://doi.org/10.2355/isijinternational.40.280

Pevida C, Arenillas A, Rubiera F, et al., 2007. Synthetic coal chars for the elucidation of NO heterogeneous reduction mechanisms. *Fuel*, 86(1-2):41-49. https://doi.org/10.1016/j.fuel.2006.07.002

Schubert H, Herrmann W, Rumpf H, 1975. Deformation behavior of agglomerates under tensile stress. *Powder Technology*, 11(2):121-131. https://doi.org/10.1016/0032-5910(75)80037-4

Teo CS, Mikka RA, Loo CE, 1992. Positioning coke particles in iron-ore sintering. *ISIJ International*, 32(10):1047-1057. https://doi.org/10.2355/isijinternational.32.1047

Waters AG, Litster JD, Nicol SK, 1989. A mathematical-model for the prediction of granule size distribution for multicomponent sinter feed. *ISIJ International*, 29(4):274-283. https://doi.org/10.2355/isijinternational.29.274

Yang YH, Standish N, 1991. Fundamental mechanisms of pore formation in iron-ore sinter and pellets. *ISIJ International*, 31(5):468-477. https://doi.org/10.2355/isijinternational.31.468

Zhao JP, Loo CE, Dukino RD, 2015. Modelling fuel combustion in iron ore sintering. *Combustion and Flame*, 162(4):1019-1034. https://doi.org/10.1016/j.combustflame.2014.09.026

Zhou H, Liu ZH, Cheng M, et al., 2015. Influence of coke combustion on NO_x emission during iron ore sintering. *Energy & Fuels*, 29(2):974-984. https://doi.org/10.1021/ef502524y

Zhou H, Cheng M, Zhou MX, et al., 2016. Influence of sintering parameters of different sintering layers on NO_x emission in iron ore sintering process. *Applied Thermal Engineering*, 94:786-798. https://doi.org/10.1016/j.applthermaleng.2015.09.059

Zhou H, Li Y, Tang Q, et al., 2017. Combining flame monitoring techniques and support vector machine for the online identification of coal blends. *Journal of Zhejiang University-SCIENCE A (Applied Physics & Engineering)*, 18(9):677-689. https://doi.org/10.1631/jzus.A1600454

中文概要

题　目： **铁矿石制粒粘附比预测及其对烧结过程中 NO_x 生成的影响**

目　的： 铁矿石烧结需要对原料进行制粒，而焦炭被细粉颗粒覆盖，会影响其燃烧。本文旨在建立制粒模型分析粘附比例和粘附层的有效面积，并研究铁矿石制粒粘附层厚度对 NO_x 生成的影响。

创新点： 1. 建立制粒模型计算多组分原料制粒的粘附比；2. 结合制粒模型计算粘附比和在不同粘附比下进行 NO_x 释放实验，并对制粒中的焦炭进行合理分布。

方　法： 1. 通过理论分析，建立原料颗粒参数与制粒粒径分布的关系（公式（1）~（11））；2. 通过实验和制粒模型分析水分以及各种原料的特性对制粒粒径分布的影响（图 4~10）；3. 通过管式炉实验分析不同粘附层厚度对 NO_x 释放的影响（图 12 和 13）。

结　论： 1. 制粒模型可以用于多组分原料的制粒粒径分布和粘附比预测；2. 粘附层对焦炭氮释放有较大影响，需要对烧结中的燃料进行合理分布；3. 通过原料成分和对粘附比的预测，可定性分析铁矿石烧结过程中 NO_x 的排放。

关键词： 铁矿石烧结；制粒；粘附层；粘附比；NO_x